Chapter 5

Laser Dissociation of Protonated PAHs

5.1 Experiments

The photodissociation experiments were performed with protonated PAHs using different laser sources. The calculations from Chapter 3 indicated that it might be energetically feasible to dissociate protonated PAHs with visible/near UV photons from the OPO in one- or two-photon process. The original goal was therefore to measure visible electronic spectra of protonated PAHs by one-photon photodissociation. Thanks to the photostability of protonated PAHs described below, a combined excimer laser and OPO experiment has been performed to yield better results.

Most experiments were performed with protonated anthracene, and some with protonated pyrene and protonated benzene. Protonated anthracene was selected as the smallest protonated PAH molecule since it had a predicted absorption in the visible wavelength region, where 355 nm -pumped OPOs have several mJ of pulse energy. Protonated pyrene is heavier and has lower vapor pressure; therefore, it was the second molecule of choice. The S_2 state of protonated benzene lies within reach of frequency-doubled BBO OPOs and its spectrum, although broad, was measured previously [90]. The S_1 state of protonated ben-

zene and protonated naphthalene, as well as neutral naphthalene, anthracene and pyrene, are all located between 300 – 400 nm and therefore, could not be accessed either by the fundamental or second harmonic of our OPO. It would be possible to generate such photons by sum frequency mixing of the OPO signal with the fundamental from the Nd:YAG laser (1064 nm) or by doubling a 532 nm pumped OPO, but neither of these methods has yet been implemented to extend the OPO wavelength range.

The single-valve hydrogen discharge source was used to protonate neutral aromatic molecules (Chapter 4, 4.2), and the delay times for the discharge and ion extraction were optimized to produce the maximum protonated ion signal. The laser delay time was then adjusted to selectively dissociate the protonated ions. The signals from both the reflectron (parent ion depletion) and linear (neutral product formation) detectors were recorded.

5.1.1 The Type II BBO OPO as a Laser Photodissociation Source

Our first attempt to the photodissociation spectrum of protonated anthracene used the signal (visible) beam from the BBO type II OPO (Chapter 4, 4.5.3). The wavelength range covered was 418 – 600 nm, with a of resolution 0.1 nm and a pulse energy from 0.3 to 5 mJ/pulse at the intersection with the ion beam. The laser beam was unfocused and had a round spot with diameter of 5 mm at $\lambda = 425$ nm and a 7×18 mm (vertical × horizontal) spot at $\lambda = 600$ nm.

No dissociation was observed for protonated anthracene. That is, the parent ion signal on the reflectron detector was within the fluctuation limits and the neutral products signal on the linear detector remained within the noise level. After this first attempt, the OPO signal beam was focused into the TOF MS chamber either into a dot with a spherical lens (fused silica, $f = 250$ mm), or into a horizontal line with a cylindrical lens (fused silica,

$f = 250$ mm) . Again, no dissociation was observed.

Finally, the OPO signal frequency was doubled (209 – 280 nm, with a resolution of 0.05 nm) to search for more highly excited states. Still, no dissociation was recorded for protonated anthracene, and a similar attempt to record the spectrum of the S_2 state of protonated benzene around 250 nm (as was found previously [90]) resulted in no observed dissociation.

5.1.2 Two-color Dissociation – OPO and Excimer Laser

The OPO scan demonstrated that more intense pulses may be needed to dissociate protonated PAHs on nanosecond timescales; therefore, the dissociation experiment was performed with pulses from two lasers. The idea was to perform $1 + 1'$ resonance-enhanced multiphoton dissociation. The first photon (1) from the OPO (visible wavelengths) would excite the protonated PAH ion electronically. Then, the second photon ($1'$) from the excimer laser ($\lambda = 193$ nm) would provide the additional energy needed to dissociate the excited ion. The excimer pulse energy was kept below ∼10 mJ/pulse to ensure that the dissociation was produced by both lasers and not the excimer laser alone. The pulse duration for the OPO was ∼2.5 – 3.5 ns while that for the excimer laser was 20 ns. The time delay between the two lasers was synchronized with a fast photodiode, and set either to have the OPO pulse arrive 1 ns ahead of the excimer pulse or during its maximum intensity. As in the case of the OPO only scans, the neutral fragment signal did not depend on the OPO wavelength and thus, no $1 + 1'$ protonated anthracene dissociation was observed.

5.1.3 Dissociation Yield with Excimer Laser

In order to better understand the lack of dissociation in the OPO and OPO with excimer experiments, additional high energy excimer studies at $\lambda = 193$ and 248 nm were performed on protonated anthracene, pyrene and benzene. Good depletion signals were observed once the delay time of the laser was set in order to dissociate ions of the appropriate mass. Typical mass spectra for protonated pyrene (Figure 5.2), protonated anthracene (Figure 5.1) and the neutral product from protonated anthracene (Figure 5.3) are shown below. Figure 5.4 demonstrates that the neutral product signal arises from protonated anthracene dissociation because it has the same flight time as the parent ion in the linear TOF MS mode. A strong and narrow peak was produced on the linear detector (neutral channel) by the excimer laser and was not RF induced (Figure 5.3). This peak was present even when there were no ions (that is, with the discharge turned off) and it moved in time when the laser delay was changed, but disappeared when the beam was blocked. No signal was produced by UV photons striking the reflectron detector or by visible photons on either detector.

The dependence of the dissociation yield on the UV pulse energy was measured for protonated anthracene and protonated pyrene by recording the signal at every laser intensity with the laser ON and OFF (blocked beam) for normalization purposes. The laser delay was chosen to maximize the depletion of the parent ion peak in the mass spectrum, and the signals from both reflectron and linear detectors were recorded. When the data were plotted, the curves for parent ion depletion and neutral products showed similar behavior, but the neutral products data were less noisy and therefore used in the subsequent analysis.

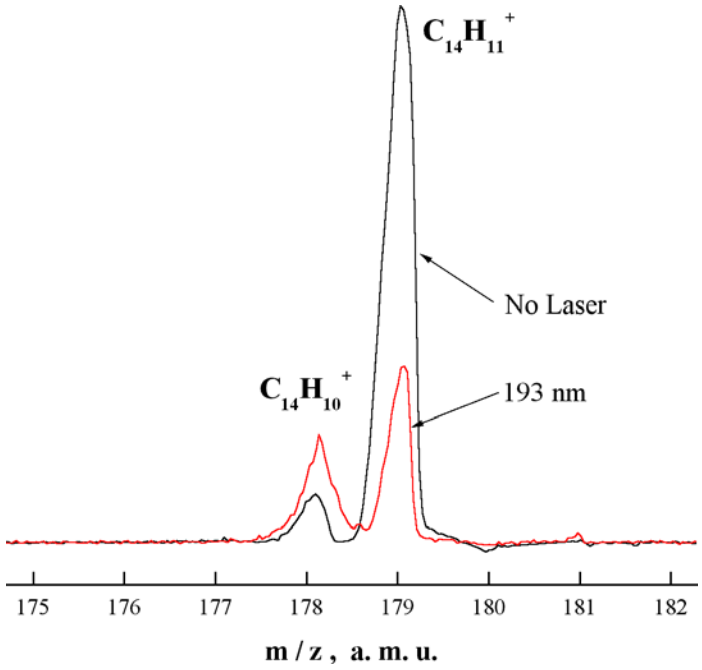

Figure 5.1: An ion channel mass spectrum of protonated anthracene photodissociation with $\lambda = 193$ nm excimer laser pulses.

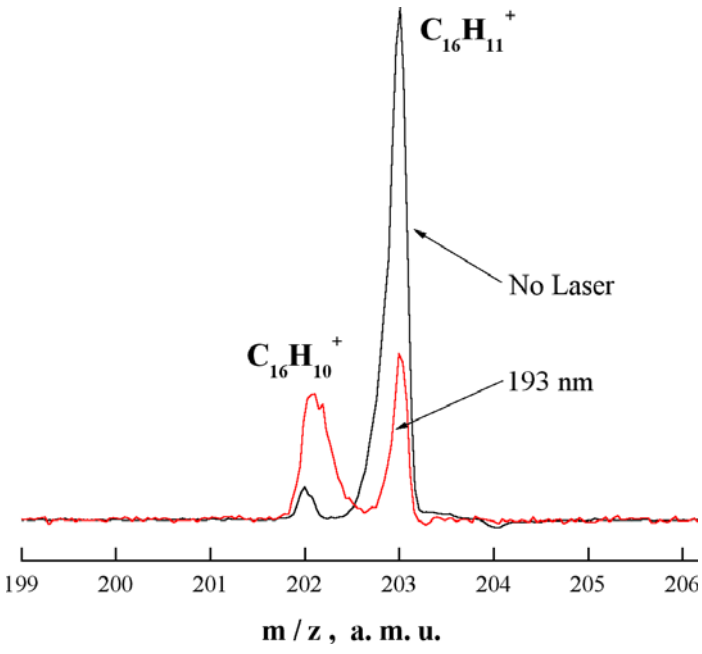

Figure 5.2: An ion channel mass spectrum of protonated pyrene photodissociation with $\lambda = 193$ nm excimer laser pulses.

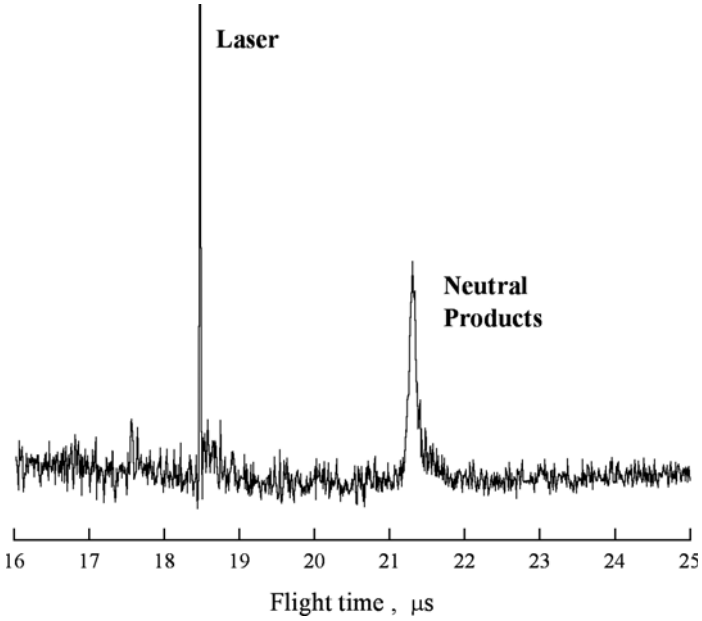

Figure 5.3: Mass spectrum of the neutral products from protonated anthracene photodissociation.

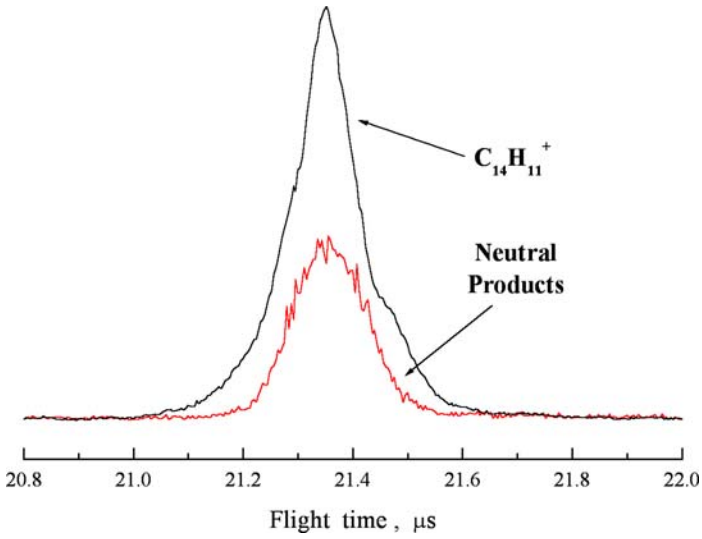

Figure 5.4: Comparison of the linear mode mass spectra for protonated anthracene and its neutral photodissociation products.

5.2 Observed Results

Under our experimental conditions, protonated anthracene and protonated benzene did not dissociate from low energy (<10 mJ/pulse) pulses produced by nanosecond visible and UV lasers. However, all studied ions (protonated anthracene, protonated pyrene and protonated benzene) dissociated after interaction with $10 \leq E \leq 35$ mJ pulses. This implies the dissociation is multiphoton in nature.

5.2.1 Photodissociation Products

No experiments were conducted to determine the exact nature of the neutral photodissociation products, although some information may be derived from the ion mass spectra in the reflectron channel. Ground state DFT calculations (Chapter 2) have shown that the two lowest dissociation channels should be the loss of a hydrogen atom or the hydrogen molecule, and so these are expected to be the primary neutral dissociation products. Primary ion dissociation products (the cation and dehydrogenated cation) may undergo further dissociation in intense laser fields. Since the laser intercepts the ion beam before it enters the reflectron, only neutral products can pass through the reflectron to produce the signal on the linear detector. The ion dissociation products (ions with positive charge), however, cannot penetrate the reflectron and are deflected toward the reflectron detector. Ions from fast dissociation with small recoil velocities will be collected efficiently by the reflectron and produce reasonably narrow enough mass peaks at the reflectron detector.

The only observed changes in the ion mass spectrum under high intensity laser pulses were the decrease in the intensity of the parent ion peak for protonated PAHs ($m/z = M + 1$) and a concomitant increase in the intensity of the cation peak ($m/z = M$) (see Figures 5.1, 5.2). No other new peaks appeared in the mass spectrum when the laser was used.

The decrease in the parent ion peak intensity is due to protonated PAH dissociation, and can be as high as 90%. The complete depletion of this peak depends on the spatial overlap of the laser beam with the mass M + 1 ion packet and may be less than 100%. The intensity increase in the cation peak is significantly smaller than the observed protonated ion loss. This suggests that either the dissociation is not sufficiently prompt or that secondary, tertiary, etc. dissociations are possible. One way to test this idea would be to intercept the ions as soon as they are extracted into the mass spectrometer field-free flight region. Unfortunately, this has to be done very close to the reflectron detector which is saturated by the scattered UV light from the laser for an extended time period (more than 100 μs), making it impossible to draw a conclusion. On the other hand, the neutral products signal changes with laser intensity. This may mean that the dissociation is sufficiently fast for the neutral products to be concentrated into a small solid angle.

The intensity increase in the cation peak does not mean that the dissociation happens through the H atom loss channel. In fact, it indicates that the primary dissociation channel is the loss of an H_2 molecule (or two H atoms). This is due to the fact that the dissociation occurs approximately in the middle of the ion flight. In this case, the ions that produce the additional cation signal have mass M + 1 before dissociation (about half of the flight time) and mass M – 1 after (second half of the flight), averaging to mass M. For the H atom loss channel, the ion peak shift would be only 0.5 a.m.u., not the observed 1 a.m.u. The shift would be 2 a.m.u. if the dissociation was performed immediately after the ions were extracted into the mass spectrometer from the discharge.

The loss of two H atoms or the H_2 molecule is in good agreement with the previously observed products in the photodissociation of protonated benzene [90] and the coronene cation [120].

5.2.2 Yield Dependence on the Pulse Energy

In general, photodissociation product yields with respect to the light intensity (pulse energy) can be expected as a power law relationship with exponent γ:

$$S \propto I^{\gamma}$$

The slope of the S *vs.* I curve on a log–log plot gives γ, which corresponds approximately to the number of photons in the process. Data for the photodissociation of protonated anthracene with 193 and 248 nm photons are plotted in Figures 5.5 and 5.6, those for

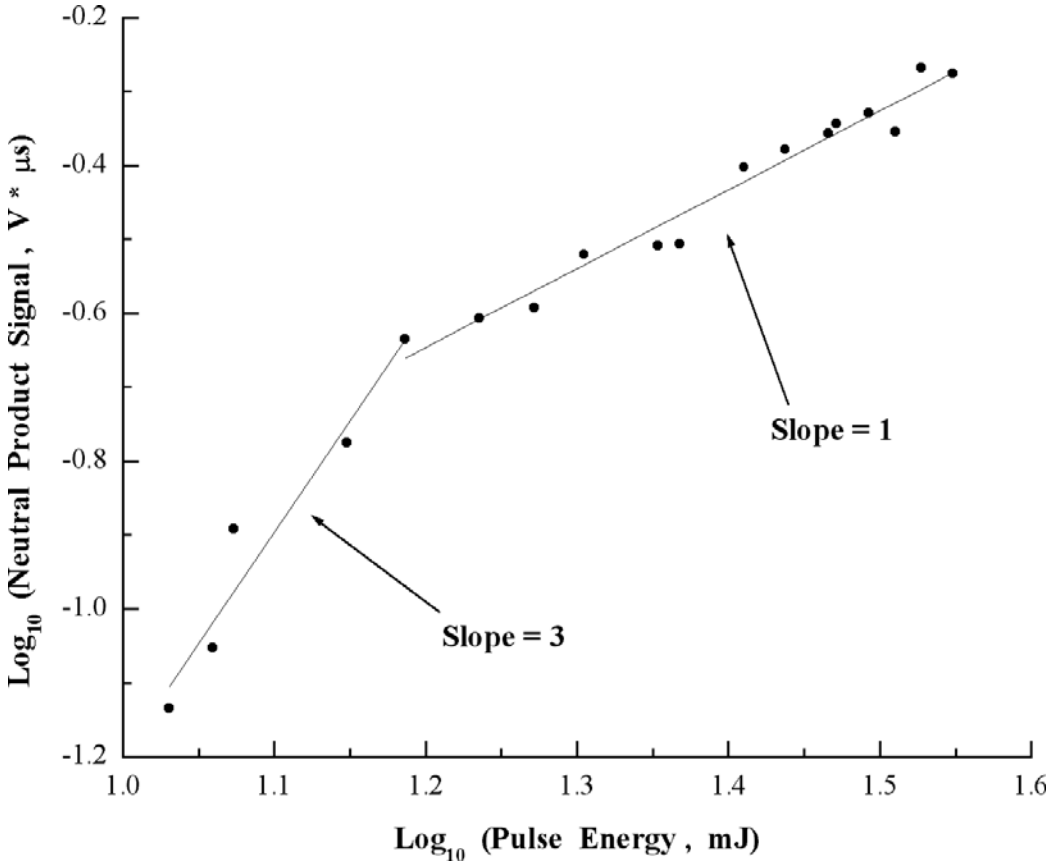

Figure 5.5: Protonated anthracene photodissociation with $\lambda = 193$ nm excimer laser pulses. The dependence of neutral products yield on the pulse energy is indicated by the linear fits in this and subsequent log-log plots.

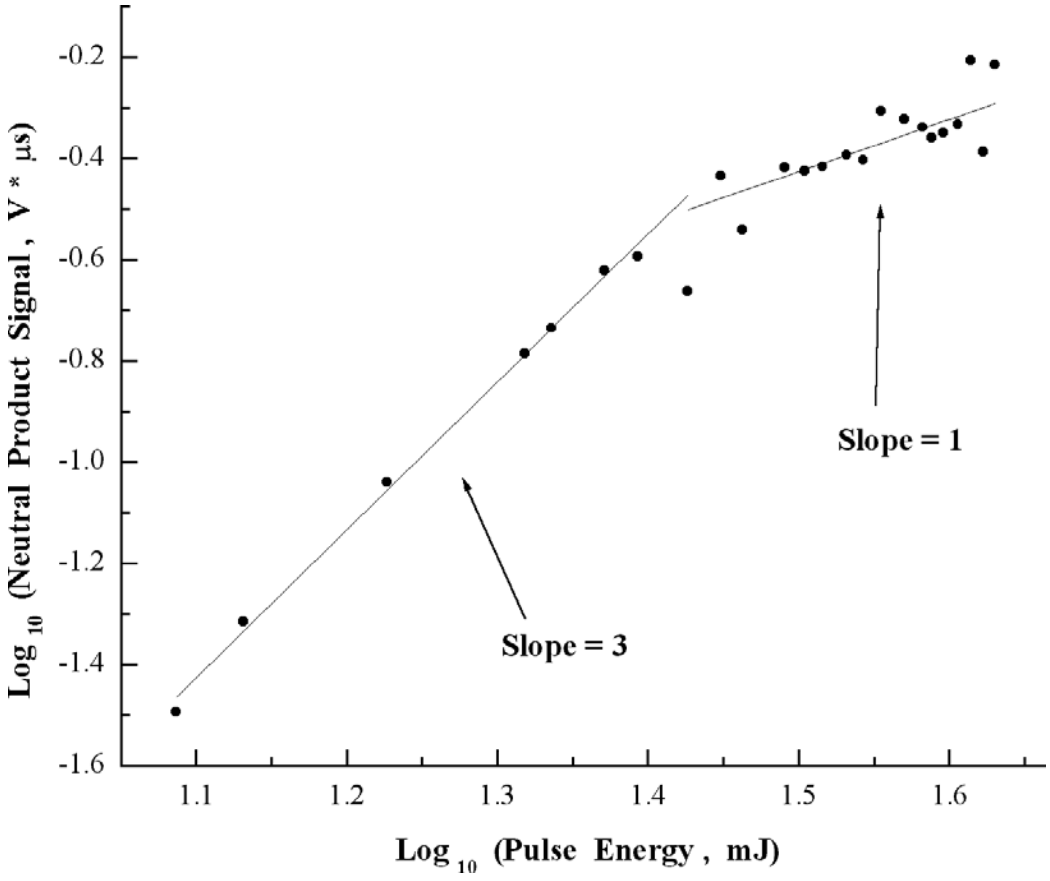

Figure 5.6: Protonated anthracene photodissociation with $\lambda = 248$ nm excimer laser pulses.

protonated pyrene with 193 nm photons in Figure 5.7.

At low pulse energies, the curves for protonated anthracene have a slope of 3. This means that nonresonant dissociation at both 193 and 248 nm is a three-photon process. Both curves have a slope of 1 at higher pulse energies due to the saturation of some of the dissociation steps.

For protonated pyrene, the slope at low intensities was 11. There were two reasons for this unphysical result. First, the pulse energy fluctuations were quite high in this experiment, increasing the uncertainty. Second, protonated pyrene clearly dissociates noticeably easier than does protonated anthracene. This indicates that the transition to one of its

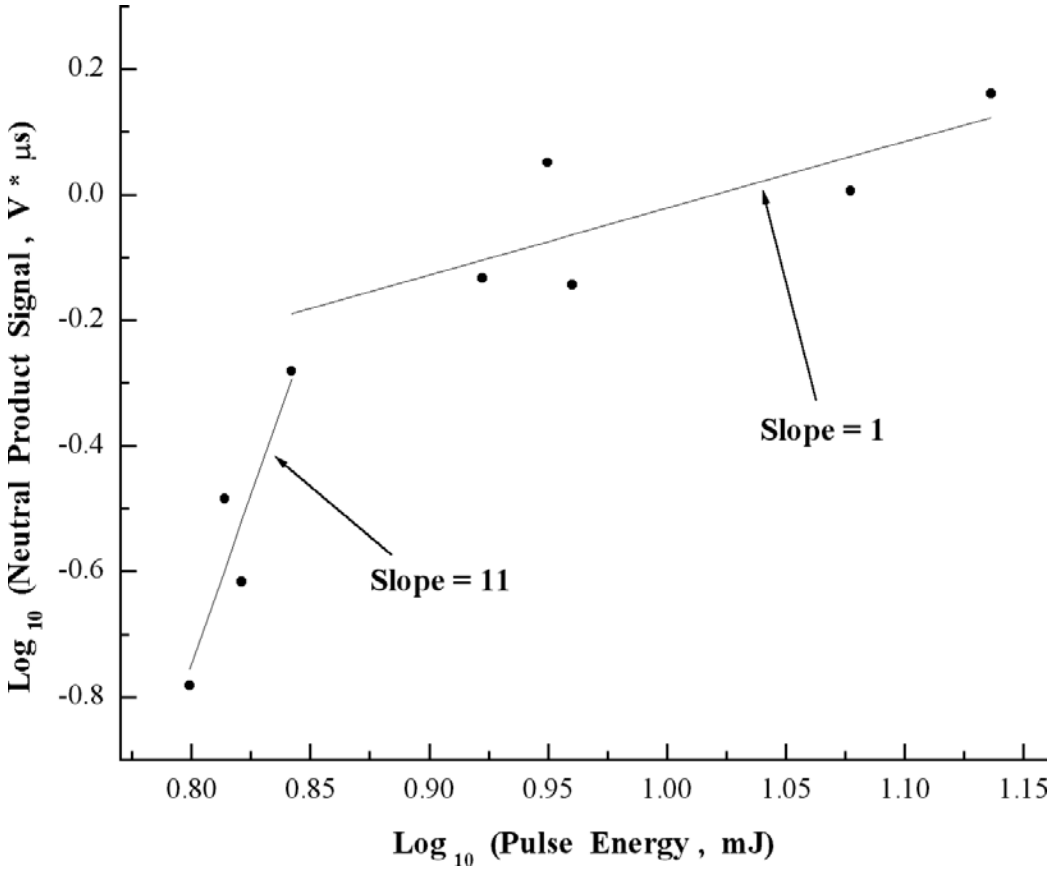

Figure 5.7: Protonated pyrene photodissociation with $\lambda = 193$ nm excimer laser pulses.

excited states lies close to 193 nm, and that the dissociation efficiency was influenced by the proximity to a resonance. The overall nature of dissociation was still multiphoton, but the direct relationship of the slope to the number of photons needed no longer applies.

The observed behavior for protonated benzene was similar to protonated anthracene, although the detailed dissociation yield versus energy was not measured accurately.

5.3 Discussion

5.3.1 Multiphoton Nature of the Photodissociation

The excimer experiments show that the UV photodissociation of protonated PAHs is clearly multiphoton. For protonated anthracene, it is possible to estimate the internal energy required for dissociation (Figure 5.8). Since both 193 and 248 nm dissociation is a three photon process, protonated anthracene dissociates rapidly after absorbing three photons, but not from two photons. Three 248 nm photons therefore establish the upper limit for the dissociation energy while two 193 nm photons determine the lower limit.

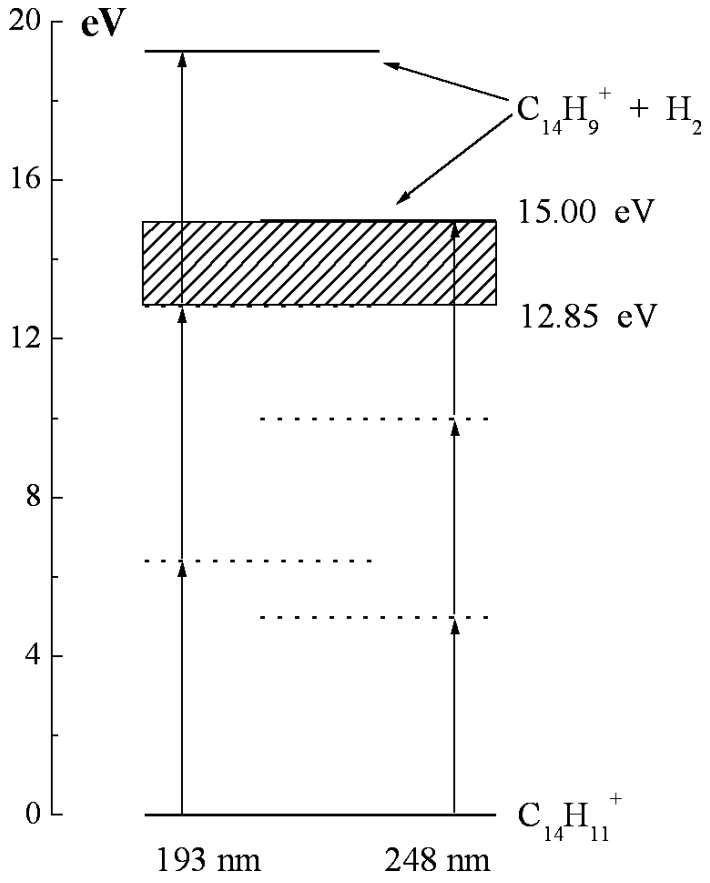

Figure 5.8: Estimates of dissociation energy for protonated anthracene by multiphoton nanosecond laser excitation.

Thus, when using a nanosecond laser, one needs to place 12.85 – 15.00 eV (296.3 – 345.9 kcal/mol) of internal energy into the protonated anthracene ion for it to dissociate in these nanosecond experiments. This is the total amount of energy required and not that needed thermodynamically to break the bonds. Indeed, it is much higher than the dissociation energies (60 – 70 kcal/mol) calculated in Chapter 2. The excess energy goes mostly into the vibrational degrees of freedom of the products, especially in the heavy ion produced. Intramolecular vibrational energy redistribution (IVR) plays a crucial role here.

Two-photon dissociation has been observed in the dissociation of the benzene [149] and naphthalene [67] cations. Here, IVR was also seen to lead to the broadening of the absorption bands in the spectrum. The spectral broadening grew very fast with the number of vibrational modes in the molecule and similar effects may make it impossible to record the photodissociation spectra of large PAHs or PAH cations.

A picture of the dissociation that explains the experimental results is as follows: photons are absorbed quickly during the laser pulse (a few nanoseconds) simultaneously, sequentially, or a combination of both. Then, an electronically excited molecule returns to the ground electronic state potential energy surface via internal conversion and IVR, in the process becoming vibrationally excited. The vibrational energy is distributed over the many different vibrations in the molecule. When the vibrational excitation is sufficiently high, the molecule dissociates. For protonated anthracene, this requires on the order of 4.6 kcal/mol (1620 cm^{-1}) per vibrational mode, which is calculated by dividing the estimated dissociation threshold by the total number of vibrational modes.

This explains why one-photon and $1 + 1'$ two-photon dissociation was not observed with lower energy laser pulses. For example, the dissociation of protonated anthracene with visible nanosecond pulses would be a five-photon process. To observe any noticeable

dissociation signal with the visible wavelength photons, the light intensity needs to be much higher than was available here. Such intensities are achievable using much shorter pulses (picosecond or femtosecond duration), but it is not possible to produce enough energy with widely tunable nanosecond lasers (OPOs, dye, etc.) such as those used in the current setup.

To circumvent such pulse energy limitations with high spectral resolution lasers, the experiment needs to be modified. One possibility is to increase the interaction time of the ions with laser radiation by placing the ions into a trap. Photodissociation experiments of this type used a FT ICR trap for protonated benzene [90] and the coronene cation [120], and an RF trap for the anthracene and phenanthrene cations [138]. Alternatively, clusters of protonated PAHs with rare gas atoms or volatile molecules can be made. In this case, the approach would be to measure the one-photon dissociation spectrum of the cluster. This approach is described in Chapter 6 for the specific case of clusters of protonated anthracene with water.

5.3.2 Photostability and Implications for ISM

The observed photostability of protonated PAHs makes it very difficult to record their electronic absorption spectra in TOF systems. On the other hand, this is a very good argument towards the existence of protonated PAHs in the interstellar medium. The ground state calculations described in Chapter 2 have shown that if PAHs exist in the ISM, at least a sizable fraction would exist in the protonated form. The calculations for the excited states from Chapter 3 predict that most protonated PAHs will absorb in the visible and near-UV regions. Our attempts to record photodissociation spectra of protonated PAHs demonstrate that they are extremely resilient against single visible and UV photon dissociation

The estimated single photon dissociation energy of protonated anthracene is close to 13.6

eV. Thanks to the high abundance of hydrogen in a gas of solar composition, most radiation with photon energies above 13.6 eV is absorbed by the ISM and hence is unavailable to dissociate or ionize atoms and molecules. If species do not dissociate through photons with wavelength longer than 912 Å, they are photostable in the ISM. The radiation fluxes in interstellar clouds are not nearly sufficient for multiphoton absorption to occur.

Thus, should protonated PAHs exist in the diffuse ISM, their life cycle would be as follows. An ion in the ground state absorbs a visible or UV photon; it does not dissociate but rather, becomes vibrationally excited. The excess vibrational energy is then emitted at IR wavelengths over a period of milliseconds to seconds, the radiative lifetime for vibrational states. Cold ions can cycle through this loop for long time, and since the UV photon absorption interval is much larger than the IR emission lifetime, most protonated PAHs will exist in their ground states. Such a picture is in perfect agreement with the theory that PAHs (or protonated PAHs) are the species that emit the 3.3 – 11.3 μm UIRs. The question of whether protonated PAHs are DIB carriers still remains to be answered.

Removal mechanisms for protonated PAHs in the ISM include the absorption of more than one photon (highly unlikely), undergoing a chemical reaction, neutralization by dissociative electron recombination, or destruction by high energy particles (e.g. cosmic rays).

5.4 Summary

Several attempts were made to record single- and two-color visible and UV photodissociation spectra of protonated PAHs, but were not successful. Protonated PAHs were found, however, to dissociate under sufficiently intense UV laser pulse excitation. The photodissociation yield measurements demonstrate that nanosecond dissociation is multiphoton in nature. For protonated anthracene, dissociation is a three-photon process at 193 and 248

nm.

The photodissociation energy of protonated anthracene was estimated to be 12.85 – 15.00 eV, a value much higher than the thermodynamic threshold predicted in calculations reported in Chapter 2. Thus, even small protonated PAHs are very photostable, likely due to rapid IVR in the excited states.

This pronounced photostability of protonated PAHs argues in favor of their existence in interstellar clouds.